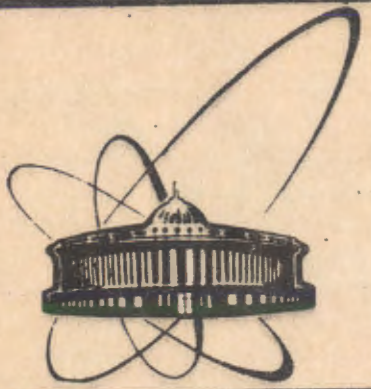

объединенный
институт
ядерных
исследований
дубна

E8-91-452

V.N.Trofimov, V.M.Drobin

A SIMPLE PORTABLE SQUID-BASED SUSCEPTOMETER

Submitted to the International Cryogenic Engineering Conference ICEC-92, Kiev, June 8-12, 1992

1991

1. Introduction

The semileptonic decays of mesons are a source for the determinaition of the Kobayashi-Maskava (KM) matrix elements from the comparison of theoretical description and the experimental data. The main theoretical uncertanties in understanding the semileptonic decays arise from the matrix element of the weak current between meson states. Many theoretical models have been used to calculate this matrix element and the semileptonic decay widths [1-9]. Recently the new detailed experimental data on the width and form factors of the decay $D \to K^* \ell \nu_\ell$ was presented by the E691 collaboration [10]. This data contrudicts almost all the predictions of the theoretical models [1-9]. One of the origins of the discrepancy may be in the neglection of the relativistic effects.

In this paper we calculate the semileptonic decay widths and form factors in the framework of the relativistic quark model based on the quasipotential method. This model has been used for the calculations of the quarkonium mass spectra [11], radiative decay widths [12] and pseudoscalar decay constants [13].

2. Semileptonic decays of mesons

The transition amplitude for the exclusive semileptonic decay $B \to A \ell \nu_\ell$ is

$$A(B \to A \ell \nu_\ell) = \langle A \ell \nu_\ell | H_{eff} | B \rangle = (G_F/\sqrt{2})\, V_{ab}\, L_\mu H^\mu ; \qquad (1)$$

where $$H_{eff} = (G_F/\sqrt{2})\, J^\mu_{hadron} J_{lepton,\mu} ; \qquad (2)$$

$$L^\mu = \bar{\ell} \gamma^\mu (1-\gamma_5) \nu_\ell \qquad (3)$$

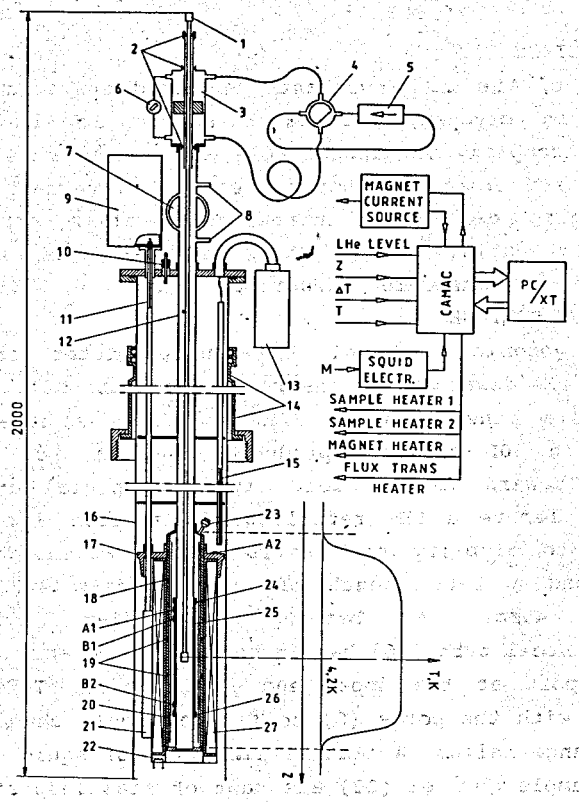

Fig.1. Schematic illustration of a squid-based susceptometer. (1)-sample holder, (2)-sliding seals, (3)-cylinder with water-glycerin solution, (4)-poppet valve, (5)-pump, (6)-bypass, (7)-gate valve, (8)-recovery ports, (9)-squid RF unit, (10)-electrical connection, (11)-coaxial feeder, (12)-sample channel tube, (13)-thermocouple amplifier and LHe level-gauge electronics, (14)-sluice chamber, (15)-LHe level-gauge sensor, (16)-bearing tube, (17)-flange, (18)-copper tube, (19)-pick-up coils, (20)-radiation screen, (21)-squid magnetic shield, (22)-heat switch, (23)-leak-tight wires inlet, (24)-upper heater, (25)-copper sample chamber, (26)-lower heater, (27)-superconducting magnet, A1,2 and B1,2 -sensing ends of thermocouples.

chamber (25), is made of OFHC copper. Heaters (24) and (26) are wounded in their upper and lower ends. The chamber temperature is measured by two Cu:Fe/Chromel thermels with sensing ends indicated as A1,2 and B1,2. Thermocouple B with the heater (26) minimizes temperature gradient along the chamber and thermocouple A with the heater (24) monitores its absolute temperature. The chamber is surrounded with a vacuum space formed by a copper tube (18) which is a frame of the astatic pick-up coils (19) of the superconducting flux transformer. The thermels and the heaters are sealed with a low temperature epoxy seal (23). The chamber has an upper and a lower thermal contacts with LHe via stainless-steel tubes 5.0·0.3mm and thus a longitudinal heat leak from the warm part of the insert is exluded. The temperature distribution at the channel for T»4.2K is shown at riht part of Fig.1. The thermal contact of the sample with chamber walls is exellent in a wide range of exchange gas pressure. A superconducting magnet (27) with a heat switch (22) has a common axis with the chamber. RF squid is placed inside a superconducting shield (21). The bottom of the insert can be placed in a hermetically sealed space formed by a stainless-steel can (not shown) and by a flange (17). The seal is provided by conical contact surfaces greased with Apiezon N. But in this case a symmetry in thermal exchange of the chamber with LHe is lost and an overheating of the magnet lower end is observed when T>90K. From the other hande we are convinced of a stable squid operation in LHe for many years if its warming to room temperature is carried out in a helium vapour. For this purpose there is a sluice chamber (14) mounted at a top of the dewar which ensures fast warming of the insert lower end. Warming from 4.2K to room temperature during 30min is possible if a gas burner is used. Instead of the above mentioned hermetical can the insert end can also be surrounded with a ferromagnetic or a superconducting magnetic shield but their use leads to remanent magnetic field origin after a strong field operation. In the case of low magnetic noise the magnetic shield can be removed as the additional magnetic filters (not shown) sufficiently lower the external influence on pick-up coils. Because of lack of space and in order to symplify the design a superconducting tube for field trapping

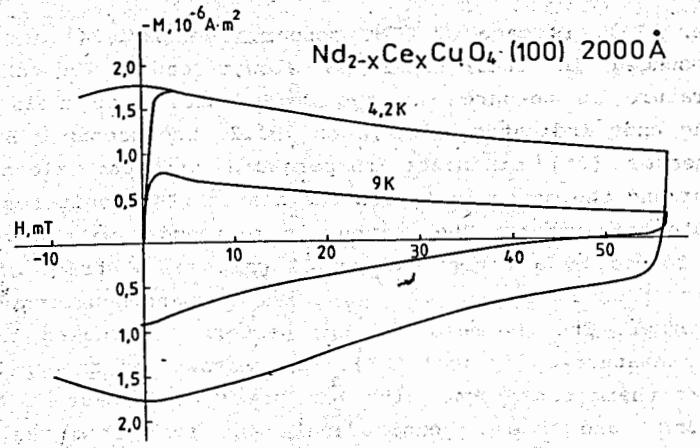

Fig.2. Magnetization hysteresis loops of epitaxial $Nd_{2-x}Ce_xCuO_4$ (x=0.15) film in a transverse field H⊥c-axis.

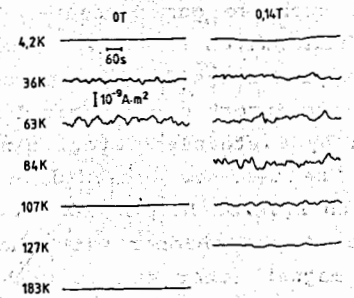

Fig.3. Output squid voltage vs time at various temperatures and two values of applied field.

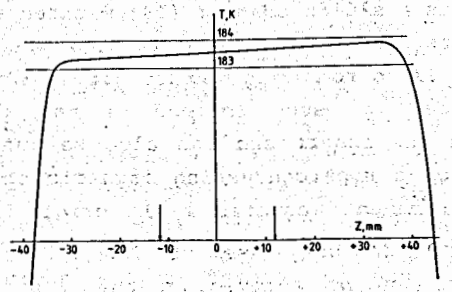

Fig.4. Temperature distribution in sample channel. Arrows show pick-up coils position.

is not used. This results in a time of the field stabilization increase for fields higher than 0.5T. LHe level is measured with a capacitive level-gauge (15)[1] with its electronics in a box (13) together with a preamplifier of the thermel A. Hermetically sealed electrical connection (10) allows to use 24 wires for thermometers and heaters. A squid RF head (9) is mounted at the top of the coaxial line.

The susceptometer is also equiped with crate CAMAC, PC/XT, magnet current source, squid control unit and two digital voltmeters to measure squid output voltage, sample position and temperature, magnetic field. CAMAC units include two temperature regulators with electrically decoupled heaters[2], DACs to control the current source and the sample temperature, level-gauge indicator, heaters control unit, voltmeter interfaces. Manual operation is possible also. The susceptometer was successfully used without any shock insulation at the ground floor of the laboratory building.

3.TECHNICAL SPECIFICATIONS

Inspite of simple design our instrument provides good performance for magnetic measurements with different samples including ferromagnetic materials and high-T_c superconducting thin films and crystals. As an example Fig.2 shows magnetization curves of a highly oriented epitaxial $Nd_{2-x}Ce_xCuO_4$ (x=0.15) film with diam=2mm in a transverse field.

The full magnetic field range is ∓1T. Field uniformity over pick-up coils distance is 0.1%. Residual field after operation at 1T is 2mT and after demagnetization cycle is 0.05mT. The ambient field after cooling can be compensated to 0.005mT using lead sample as a probe. The drift time after field change is (1-5)min at H<0.5T and (10-30)min at H>0.5T. Range of measurement is $(10^{-10}-5\cdot10^{-6})A\cdot m^2$. The resolution depends on temperature and field as is seen from Fig.3 where the output squid voltage versus time is plotted. The maximum low-frequency magnetic noise is observed near 90K. Temperature range is (4.2-300)K. Thermocouple A was calibrated at helium and nitrogen temperatures against two Ge thermometers mounted at the sample position. Temperature accuracy of a sample is 0.5K with resolution 0.1K. Temperature uniformity over input coils distance is better than 0.2K at 200K level. At Fig.4 an

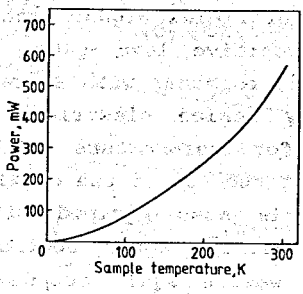

Fig.5. Total electrical power vs sample temperature.

example of temperature distribution in sample space is plotted. The sensing coils positions are indicated with arrows. Rate of temperature change is (1-15)min depending on initial and final temperatures. Fig.5 shows a power versus operating temperature. The cooldown time of the insert from room to helium temperature is 1.5 hours. Time of continuous operation with 50l of LHe is (5-6) days.

4.CONCLUSION.

Half a year operation of described susceptometer confirms the expected advantages and at the same time shows a simple way to expand the field range to (2-3)T and operating time to (9-10) days as well as to improve some design features.

REFERENCES

1.I.Velitchkov, V.Drobin, JINR 8-88-213 Dubna, 1988.

2.The electronics was designed by I.Velitchkov from the University of Sofia, Bulgaria.

Received by Publishing Department
on October 17, 1991.

$$H^{\mu}=<A|\bar{a}\gamma^{\mu}(1-\gamma_5)b|B> \quad ; \qquad (4)$$

V_{ab} is the corresponding KM-matrix element, B is the initial pseudoscalar meson, A is the final pseudoscalar (vector) meson.

The hadronic matrix element (4) is usually decomposed in invariant form factors [3,4,5] defined by :

a) for the decay to the pseudoscalar meson $B_{\ell}\to A\ell\nu_{\ell}$

$$<A(p_A)|J^V_{\mu}|B(p_B)>=f_+(q^2)(p_A+p_B)_{\mu}+f_-(q^2)(p_B-p_A)_{\mu} \quad ; \qquad (5)$$

b) for the decays to the vector meson $B\to A^*\ell\nu_{\ell}$

$$<A^*(p_A,e)|J^V_{\mu}|B(p_B)>=ig(q^2)\varepsilon_{\mu\nu\rho\sigma}e^{*\nu}(p_B+p_A)^{\rho}(p_B-p_A)^{\sigma}; \qquad (6)$$

$$<A^*(p_A,e)|J^A_{\mu}|B(p_B)>=f(q^2)e^*_{\mu}+a_+(q^2)(e^*p_B)(p_A+p_B)_{\mu}+$$

$$+a_-(q^2)(e^*p_B)(p_B-p_A)_{\mu}; \qquad (7)$$

where $q=p_B-p_A$; $J^V_{\mu}=(\bar{a}\gamma^{\mu}b)$ and $J^A_{\mu}=(\bar{a}\gamma^{\mu}\gamma_5 b)$ are the vector and axial parts of the weak quark current, e_{μ} is the polarization vector of the vector meson A^*.

Since $q=p_{\ell}+p_{\nu_{\ell}}$, the terms proportional to q_{μ}, i.e. f_- and a_- give contributions proportional to the lepton masses and do not influence significantly the transition amplitude, except in the case of the heavy τ lepton.

The decay rate and differential decay rate can be calculated in terms of the invariant form factors. The formulas are [3]:

$$\frac{d\Gamma}{dy}=\frac{G_F^2|V_{ab}|^2 K M_B^2 y}{96\pi^3}\left(|H_+|^2+|H_-|^2+|H_0|^2\right) \quad ; \qquad (8)$$

where $y=q^2/M_B^2$; $K=\frac{M_B}{2}\left[\left(1-\frac{M_A^2}{M_B^2}-y\right)^2-4\frac{M_A^2}{M_B^2}y\right]^{1/2}$

For the decay to the pseudoscalar meson $B\to A\ell\nu_{\ell}$

$H_{\pm}=0$; $\quad H_0=-2Ky^{-1/2}f_+(y)$

and for the decay to the vector meson $B\to A^*\ell\nu_{\ell}$

$$H_0=\frac{M_B}{2M_A\sqrt{y}}\left(\left(1-\frac{M_A^2}{M_B^2}-y\right)f(y)+4K^2a_+(y)\right) \qquad (10)$$

$H_{\pm}=f(y)\mp 2M_BKg(y)$.

The ratio of the longitudinal and transverse decay widths is

$$\Gamma_L/\Gamma_T=\frac{\int dy|H_0(y)|^2Ky}{\int dy(|H_+(y)|^2+|H_-(y)|^2)Ky} \quad . \qquad (11)$$

3. Relativistic corrections to the form factors in semileptonic decays

In the quasipotential method the bound system is described by the wave function $\Psi_M(p)$ satisfying the qusipotential equation [14], which can be written in the local Schrödinger-like form [15]:

$$\left(\frac{b^2(M)}{2\mu_R}-\frac{p^2}{2\mu_R}\right)\Psi_M(p)=\int\frac{d^3q}{(2\pi)^3}V(p,q;M)\Psi_M(q) \quad ; \qquad (12)$$

where the relativistic reduced mass is

$$\mu_R=\frac{E_1E_2}{E_1+E_2}=(1/4M^3)[M^4-(m_1^2-m_2^2)^2]; \qquad (13)$$

$$E_1=\frac{M^2-m_2^2+m_1^2}{2M} \quad ; \quad E_2=\frac{M^2-m_1^2+m_2^2}{2M} \quad ; E_1+E_2=M \; ;$$

the square of the relative momentum p on the mass-shell is equal to

$$b^2(M)=[M^2-(m_1+m_2)^2][M^2-(m_1-m_2)^2]/4M^2 \qquad (14)$$

m_1, m_2 are the quark masses; M is the meson mass.

To constract the kernel of this equation V(p,q,M)-the quasip o tential-we assume that effective quark-antiquark interaction is the mixture of the single gluon exchange with the long-range vector and scalar linear confining potentials. We

also assume that quarks have an anomalous chromomagnetic moments κ.

Then the quasipotential is

$$V(p,q;M)=\bar{u}_1(p)\bar{u}_2(-p)\left\{\frac{4}{3}\alpha_s D_{\mu\nu}(k)\gamma_1^\mu\gamma_2^\nu + V^V_{conf}(k)\Gamma_1^\mu\Gamma_{2;\mu} + V^S_{conf}(k)\right\} u_1(q)u_2(-q), \quad (15)$$

where $k=p-q$; $D_{\mu\nu}(k)$ is the gluon propagator, $u_{1,2}(p)$ are the Dirac spinors; the effective long-range vector vertex is

$$\Gamma_\mu(k)=\gamma_\mu+\frac{i\kappa}{2m}\sigma_{\mu\nu}k^\nu$$

The vector and scalar confining potentials in configuration space are

$$V^V_{conf}(r)=(1-\varepsilon)(Ar+B)$$
$$V^S_{conf}(r)=\varepsilon(Ar+B) \quad (16)$$

The explisit expression for the quasipotential with the account of the relativistic corrections of order v^2/c^2 can be found in [11]. The method of the numerical solution of (12) was described in [16].

The matrix element of the local current J between bound states [17,18] has the form

$$\langle A|J_\mu(0)|B\rangle=\int\frac{dp\,dq}{(2\pi)^6}\bar{\Psi}_A(p)\Gamma_\mu(p,q)\Psi_B(q), \quad (17)$$

where $\Gamma_\mu(p,q)$ is the two-particle vertex function.

In our case $J=J^A+J^V$ is the weak quark current and to calculate its matrix element between meson states it is necessary to consider the contributions to Γ from the diagrams on figs.1,2. The vertex functions obtained from these diagrams are

$$\Gamma^{(1)}_\mu(p,q)=\bar{u}_a(p_1)\gamma^\mu(1-\gamma_5)u_b(q_1)(2\pi)^3\delta(p_2-q_2) \quad (18)$$

and

$$f_{+S}^{(2)}(y_{max})=\sqrt{M_A/M_B}\int\frac{d^3p}{(2\pi)^3}\bar{\Psi}_A(p)\Big\{-\frac{M_B-M_A}{2m_a}\Big(\frac{M_B-\varepsilon_b(p)-\varepsilon_q(p)}{m_a}\Big)+$$

$$+\frac{M_B-M_A}{12m_a}p^2\Big(1/m_a^2+1/m_b^2\Big)-\frac{M_B-M_A}{12}\Big(1/m_a^2+1/m_b^2\Big)\Big(M_B+M_A-\varepsilon_b(p)-\varepsilon_a(p)-$$

$$-2\varepsilon_q(p)\Big)\frac{\varepsilon_q(p)}{M_A}\overleftarrow{(p\partial/\partial p)}\Big\}\Psi_B(p) \qquad (22)$$

$$f_{+V}^{(2)}(y_{max})=\sqrt{M_A/M_B}\int\frac{d^3p}{(2\pi)^3}\bar{\Psi}_A(p)\Big\{\frac{M_B-M_A}{m_a}\frac{p^2}{12\mu}\Big((1+\kappa)(1/m_a-1/m_b)-$$

$$-\frac{2}{\varepsilon_q(p)+m_q}\Big)-\frac{M_B-M_A}{12}(1+\kappa)(1/m_a^2-1/m_b^2)(M_B-M_A-\varepsilon_b(p)+$$

$$+\varepsilon_a(p))\frac{\varepsilon_q(p)}{M_A}(p\partial/\partial p)+\frac{M_B-M_A}{6(\varepsilon_q(p)+m_q)\mu}\Big(M_B+M_A-\varepsilon_b(p)-\varepsilon_a(p)-$$

$$-2\varepsilon_q(p)\Big)\frac{\varepsilon_q(p)}{M_A}\overleftarrow{(p\partial/\partial p)}\Big\}\Psi_B(p) \qquad (23)$$

2) for the decay $B\to A^*\ell\nu_\ell$

$$g(y)=g(y_{max})I(y)\mathcal{F}_1(y) \qquad (24)$$

$$g_{(1)}(y_{max})=\sqrt{M_A/M_B}\int\frac{d^3p}{(2\pi)^3}\bar{\Psi}_A(p)\Big\{\frac{1}{2m_a}\Big(1-\frac{p^2}{8}\Big(5/m_a^2+1/m_b^2-2/3m_am_b\Big)-$$

$$-\frac{p^2(m_a+\varepsilon_q(p))}{12\mu M_A\varepsilon_q(p)}-\frac{p^2}{12M_A}\Big(\frac{m_b-m_a}{m_bm_a}\Big)+\frac{m_a}{3}\Big(\frac{m_b-m_a}{m_bm_a}-$$

$$-\frac{p^2}{8}\Big(1/m_a^2\Big(3/m_a-1/m_b\Big)-1/m_b^2\Big(3/m_b-$$

$$-1/m_a\Big)\Big)\Big)\frac{\varepsilon_q(p)}{M_A}\overleftarrow{(p\partial/\partial p)}\Big)\Big\}\Psi_B(p) \qquad (25)$$

$$g_{S}^{(2)}(y_{max})=\sqrt{M_A/M_B}\int\frac{d^3p}{(2\pi)^3}\bar{\Psi}_A(p)\Big\{\frac{1}{2m_a}\Big(-\frac{M_B-\varepsilon_b(p)-\varepsilon_q(p)}{m_a}+$$

$$+\frac{p^2}{6}\Big(1/m_a^2-1/m_b^2\Big)-\frac{m_a}{6}\Big(1/m_a^2-1/m_b^2\Big)\Big(M_B+M_A-\varepsilon_b(p)-\varepsilon_a(p)-$$

$$-2\varepsilon_q(p)\Big)\frac{\varepsilon_q(p)}{M_A}\overleftarrow{(p\partial/\partial p)}\Big)\Big\}\Psi_B(p) \qquad (26)$$

$$g_{V}^{(2)}(y_{max})=\sqrt{M_A/M_B}\int\frac{d^3p}{(2\pi)^3}\bar{\Psi}_A(p)\Big\{\frac{1}{2m_a}\Big(\frac{p^2}{6}(1+\kappa)\Big(1/m_a^2+1/m_b^2-$$

$$-\frac{1}{\varepsilon_q(p)\mu}\Big)+\frac{m_a}{6}(M_B-M_A-\varepsilon_b(p)+\varepsilon_a(p))(1+\kappa)\Big(1/m_a^2+1/m_b^2-\frac{1}{\varepsilon_q(p)\mu}\Big)*$$

$$*\frac{\varepsilon_q(p)}{M_A}\overleftarrow{(p\partial/\partial p)}-\frac{p^2}{6\varepsilon_q(p)}\Big(\frac{m_b-m_a}{m_b}\Big)+\frac{m_a}{6}\Big(M_B+M_A-\varepsilon_b(p)-\varepsilon_a(p)-$$

$$-2\varepsilon_q(p)\Big)\frac{2\varepsilon_q(p)}{(\varepsilon_q(p)+m_q)M_A}\Big(\frac{m_b-m_a}{m_bm_a}\Big)\overleftarrow{(p\partial/\partial p)}\Big)\Big\}\Psi_B(p) \qquad (27)$$

$$f(y)=f(y_{max})I(y)\mathcal{F}_2(y) \qquad (28)$$

$$f(y_{max})=\sqrt{4M_AM_B}\int\frac{d^3p}{(2\pi)^3}\bar{\Psi}_A(p)\Big\{1-\frac{p^2}{8\mu^2}+\frac{p^2}{6m_bm_a}\Big\}\Psi_B(p) \qquad (29)$$

$$a_+(y)=a_+(y_{max})I(y)\mathcal{F}_1(y) \qquad (30)$$

$$a_{+}^{(1)}(y_{max})=-\frac{1}{\sqrt{4M_AM_B}}\int\frac{d^3p}{(2\pi)^3}\bar{\Psi}_A(p)\Big\{\Big(1+\frac{M_A}{M_B}\Big)\Big(1-\frac{p^2}{2}\Big(\frac{1}{4\mu^2}-\frac{1}{3m_bm_a}\Big)\Big)-$$

$$-\frac{M_A^2}{m_aM_B}\Big(1-\frac{p^2}{8}\Big(5/m_a^2+1/m_b^2+2/3m_am_b\Big)-\frac{p^2}{6M_A\mu}\Big)-\frac{M_A\varepsilon_q(p)}{\mu M_B}\Big(1/3\Big(1-$$

$$-\mu\frac{p^2}{8}\Big(1/m_a^2\Big(3/m_a+1/m_b\Big)+1/m_b^2\Big(3/m_b+1/m_a\Big)\Big)\Big)+\frac{M_B-M_A}{3(m_b+m_a)}\Big(1-$$

$$-\frac{3p^2}{8}\Big(1/m_a^2+1/m_b^2\Big)\Big)\Big)\overleftarrow{(p\partial/\partial p)}\Big\}\Psi_B(p) \qquad (31)$$

$$a_{+S}^{(2)}(y_{max})=\frac{1}{\sqrt{4M_AM_B}}\int\frac{d^3p}{(2\pi)^3}\bar{\Psi}_A(p)\Big\{\frac{M_A^2}{m_aM_B}\Big(-\frac{M_B-\varepsilon_b(p)-\varepsilon_q(p)}{m_a}+$$

$$+\frac{p^2}{6}\left(1/m_a^2+1/m_b^2\right)-\frac{m_a}{6}\left(M_B+M_A-\varepsilon_b(p)-\varepsilon_a(p)-2\varepsilon_q(p)\right)\left(1/m_a^2+\right.$$

$$\left.+\ 1/m_b^2\right)\frac{\varepsilon_q(p)}{M_A}\ (p\overleftarrow{\partial}/\partial p)\Big)\Big\}\ \Psi_B(p) \qquad (32)$$

$$a_{+v}^{(2)}(y_{max})=\frac{1}{\sqrt{4M_AM_B}}\int\frac{d^3p}{(2\pi)^3}\bar{\Psi}_A(p)\Big\{\frac{M_A^2}{m_aM_B}\Big(\frac{p^2}{6}\ (1+\kappa)\left(1/m_a^2-1/m_b^2\right)+$$

$$+\frac{m_a}{6}(M_B-M_A-\varepsilon_b(p)+\varepsilon_a(p))(1+\kappa)\left(1/m_a^2-1/m_b^2\right)\frac{\varepsilon_q(p)}{M_A}\ (p\overleftarrow{\partial}/\partial p)-$$

$$-\frac{p^2}{3(\varepsilon_q(p)+m_q)\mu}+\frac{m_a}{6\mu}\Big(M_B+M_A-\varepsilon_b(p)-\varepsilon_a(p)-$$

$$-2\varepsilon_q(p)\Big)\frac{2\varepsilon_q(p)}{(\varepsilon_q(p)+m_q)M_A}(p\overleftarrow{\partial}/\partial p)\Big)\Big\}\ \Psi_B(p) \qquad (33)$$

where indexes (1) and (2) correspond to the diagrams in figs. 1 and 2, s and v -to the scalar and vector potentials of $q\bar{q}$-interaction; $\mu=m_bm_a/(m_b+m_a)$; $y_{max}=((M_B-M_A)/M_B)^2$; $(p\overleftarrow{\partial}/\partial p)$ acts on the wave function $\bar{\Psi}_A(p)$. The dependence of the form factors on the momentum transfer was found to be

$$I(y)=\int\frac{d^3p}{(2\pi)^3}\bar{\Psi}_A(p+\frac{m_q}{M_A}\Delta)\Psi_B(p) \qquad (34)$$

where $\Delta^2=(p_B-p_A)^2=(M_B^2(1-y)+M_A^2)^2/4M_B^2-M_A^2$

and

$$\mathcal{F}_1(y)=\frac{2\sqrt{2}\ M_A}{M_B[(y-\tilde{y}-M_A/M_B)^2-(M_A/M_B)^2]^{1/2}} \qquad (35)$$

$$\mathcal{F}_2(y)=2^{-1/2}\left[1+\frac{2M_A}{M_B(y-\tilde{y})}\right]^{1/2} \qquad (36)$$

where $\tilde{y}=(M_B^2+M_A^2)/M_B^2$.

The functoins $\mathcal{F}_1$ and $\mathcal{F}_2$ emerge from the lower and upper

Table 1. Comparison of experimental data on $D\to K^*e\nu_e$ semileptonic decay form factors with theoretical predictions.

Form factor	Experiment E691	Our results	IS [1]	BW [2]	GS [3]	KS [4]
$A_1(0)$	$0.46\pm0.05\pm0.05$	0.43	0.8	0.9	0.8	1.0
$A_2(0)$	$0.0\pm0.2\pm0.1$	0.29	0.8	1.2	0.6	1.0
V(0)	$0.9\pm0.3\pm0.1$	0.50	1.1	1.3	1.5	1.0

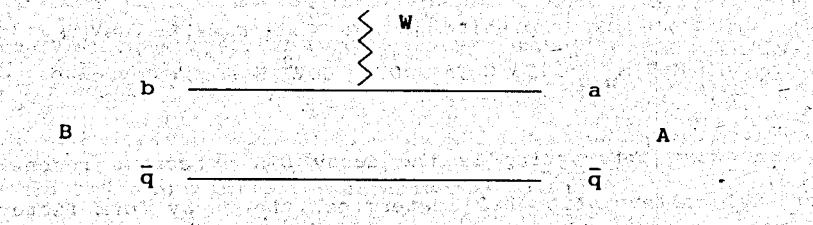

Fig.1 The lowest order vertex function.

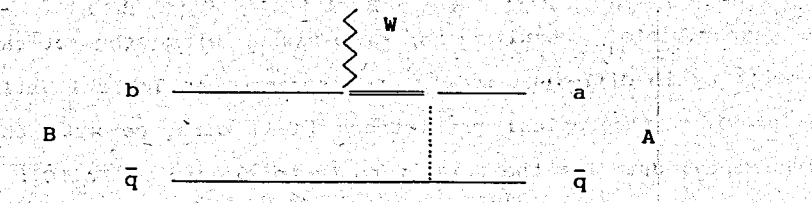

Fig.2 The vertex function with the account of the quark interaction. Dashed line corresponds to the effective potential (15). Bold line denotes the negative-energy part of quark propagator [18].

components of Dirac spinors u_a in eq.(18) respectively. We also replaced the heavy quark mass m_a by the mass of the corresponding meson M_A for simplicity.

In the limit $\omega^2/c^2 \to 0$ the form factors (20)-(33)reduce to the standard expressions , obtained in the nonrelativistic quarks models [3,5,6].

4.Results and discussion

In this section we present the results of the numerical calculations of the form factors and semileptonic decay widths of D- and B-mesons.The quark masses and parameters of the potential were determined earlier from the analysis of meson mass spectrum and radiative decays [12]: m_b=4.88 GeV, m_c=1.55 GeV, m_s=0.5 GeV, $m_{u,d}$=0.33 GeV; A=0.18 GeV^2, B=-0.30 GeV, ε=-0.9, κ =-1.

The most interesting is the decay $D \to K^* e\nu_e$ because recently the E691 collaboration [10] determined the decay form factors from the analysis of the angular correlation structure in this process. Their definition of form factors slightly differs from ours. The connection between them is the following:

$A_1(y)=f(y)/(M_A+M_B)$; $A_2(y)=-a_+(y)(M_B+M_A)$; $V(y)=g(y)(M_B+M_A)$.

The experimental results in comparison with theoretical predictions in different models are presented in Table 1.While the previous theoretical predictions [1-4] disagree with the experimental data for the axial form factors $A_1(0)$ and $A_2(0)$, we get the results in accord with these data.

For the decay width we obtain

$$\Gamma(D \to K^* e\nu_e) \tilde{=} 4.3 * 10^{10} s^{-1}$$

to be compared with the experimental data

$$\Gamma^{exp}(D \to K^* e\nu_e) = \begin{cases} (4.2 \pm 0.7 \pm 0.5) * 10^{10}\ s^{-1} & \text{(E691 [10])} \\ (3.6 \pm 0.8) * 10^{10}\ s^{-1} & \text{(PDG [19]).} \end{cases}$$

The predicted ratio of the longitudinal and transverse decay

widths is $\Gamma_L/\Gamma_T \tilde{=} 1.5$

while experimentally [10]

$$\Gamma_L/\Gamma_T = 1.8^{+0.6}_{-0.4} \pm 0.3 \quad \text{(E691).}$$

The decay width for $D \to K e\nu_e$ is predicted to be

$$\Gamma(D \to K e\nu_e) \tilde{=} 9.1 * 10^{10}\ s^{-1}$$

and the experimental data are

$$\Gamma^{exp}(D \to K e\nu_e) = \begin{cases} (8.8 \pm 1.2 \pm 1.4) * 10^{10}\ s^{-1} & \text{(E691 [20])} \\ (7.8 \pm 1.2 \pm 0.9) * 10^{10}\ s^{-1} & \text{(MARK [21])} \\ (8.1 \pm 1.2) * 10^{10}\ s^{-1} & \text{(PDG [19]).} \end{cases}$$

The form factors of the semileptonic B-meson decays have not been measured yet. Only the decay branching ratios are known.Our model predicts

$\Gamma(B \to D e\nu_e) \tilde{=} 9.0 * 10^{12} |V_{bc}|^2\ s^{-1}$ and $B(B \to D e\nu_e) \tilde{=} 10.6 |V_{bc}|^2$.

It should be comared with the experimental data

$$B(B \to D e\nu_e) = \begin{cases} (1.7 \pm 0.6 \pm 0.4)\% & \text{(ARGUS [22])} \\ \left.\begin{matrix} (1.6 \pm 0.6 \pm 0.4)\%\ D^0 \\ (1.8 \pm 0.6 \pm 0.3)\%\ D^+ \end{matrix}\right\} & \text{(CLEO [23])} \\ (1.8 \pm 0.8)\% & \text{(PDG [19])} \end{cases}$$

The prediction for the decay $B \to D^* e\nu_e$ is

$\Gamma(B \to D^* e\nu_e) \tilde{=} 2.3 * 10^{13} |V_{bc}|^2\ s^{-1}$ and $B(B \to D^* e\nu_c) \tilde{=} 27.1 |V_{bc}|^2$

and

$$\Gamma_L/\Gamma_T \tilde{=} 1.2 .$$

The experimental data are

$$B(B \to D^* e\nu_c) = \begin{cases} (5.4 \pm 0.9 \pm 1.3)\% & \text{(ARGUS [24])} \\ \left.\begin{matrix} (4.1 \pm 0.8 \pm 0.9)\%\ D^{*0} \\ (4.6 \pm 0.5 \pm 0.7)\%\ D^{*+} \end{matrix}\right\} & \text{(CLEO [23])} \\ (7.0 \pm 1.8 \pm 1.4)\% & \text{(Crystal Ball [25])} \end{cases}$$

and $\Gamma_L/\Gamma_T = \begin{cases} 0.83 \pm 0.33 \pm 0.13 & \text{(CLEO)} \\ 0.85 \pm 0.45 & \text{(ARGUS)} \end{cases}$

So we can extract the value of KM matrix element:

$$|V_{cb}| = 0.041 \pm 0.006.$$

16. V.O.Galkin, R.N.Faustov, Teor.Mat.Fiz. 85 (1990) 155

17. R.N.Faustov, Ann.Phys. 78 (1973) 176

18. R.N.Faustov, Nuovo Cim. 69 (1970) 37

19. Particle Data Group, J.J.Hernandez et al., Phys. Lett.B 239 (1990) 1

20. J.C.Anjos et al., Phys.Rev.Lett. 62 (1989) 1587

21. J.Adler et al., Phys.Rev. Lett. 62 (1989) 1821

22. H.Albreht et al., Phys.Lett.B 229 (1989) 175

23. R.Fulton et al., Phys.Rev.D 43 (1991) 651

24. H.Albreht et al., Phys.Lett.B 197 (1987) 452

25. D.Antreasyan et al., Z.Phys.C 48 (1990) 663

Received by Publishing Department
on October 16, 1991.